

# Eccentric Dynamical Tides

Yubo Su<sup>1</sup>, Dong Lai<sup>1</sup>

<sup>1</sup> *Cornell Center for Astrophysics and Planetary Science, Department of Astronomy, Cornell University, Ithaca, NY 14853, USA*

Accepted XXX. Received YYY; in original form ZZZ

## ABSTRACT

Massive stars in eccentric binaries are very important, being the progenitors of neutron star and high-mass X-ray binaries. In such systems, dynamical tides plays a crucial role. However, previous studies of dynamical tides in massive stellar binaries have primarily focused on the case where these binaries are circular. In this work, we revisit the effect of dynamical tides in eccentric, massive stellar binaries and derive analytical expressions that can be used to study binary evolution with arbitrary eccentricities. We apply our results to the radio pulsar J0045–7319, which has a massive B star companion and whose orbital period is rapidly decreasing. In order to reproduce this orbital decay via dynamical tides, we find that the core is likely rotating significantly faster than the measured surface rotation rate. This implies a long core-envelope coupling timescale in B stars.

**Key words:** keywords

## 1 INTRODUCTION

In the course of their evolution, massive stellar binaries give rise to many astrophysical systems of interest including high mass x-ray binaries (HMXRBs) and compact object binaries (CITATION with evolutionary pathway). In general, the more massive star undergoes a supernova before its less massive companion, after which the binary consists of one massive star and one compact object in an eccentric orbit (MS-CO binary). In such a system, the evolution is dominated by the torque from the compact object on the massive star due to dynamical tides. While this tidal torque is now well understood for circular binaries (Kushnir et al. 2017), it has not been carefully studied for binaries with substantial eccentricities. The tidal evolution of such eccentric binaries sculpt the population of HMXRBs (CITE) as well as the population of compact object binaries (Vigna-Gómez et al. 2020).

The dissipation due to the dynamical tide in a massive star’s envelope under the influence of a *circular* perturber is traditionally understood via Zahn’s parameterized theory of dynamical tides (Zahn 1975). However, Zahn’s theory relies on a dimensionless parameter  $E_2$  reflecting the detailed stellar structure that varies over many orders of magnitudes for typical stars. In general, the value of  $E_2$  is taken from empirical fits to simplified stellar models (Hurley et al. 2002; Vigna-Gómez et al. 2020). The introduction of this uncertain parameter  $E_2$  is because the dynamical tidal torque arises due to excitation of internal gravity waves at the radiative convective boundary (RCB) (Goldreich & Nicholson 1989; Savonije & Papaloizou 1983), but Zahn’s formula is evaluated at the *stellar* radius. Instead, it is possible re-express the tidal torque in terms of quantities evaluated at the RCB itself, for which dimensionless parameters are generally of order unity for a wide range of stars (Kushnir et al. 2017). However, Kushnir et al. (2017) only consider circular binaries.

To study the dynamical tide in eccentric binaries, it is natural to decompose the perturbing potential into Fourier harmonics, each of which is analogous to a perturber on a circular orbit (e.g. Storch & Lai 2013; Vick et al. 2017). While accurate, such decompositions

are unwieldy to evaluate as the eccentricity increases, often requiring summing hundreds of terms and lending little intuition to the broad scalings of the tidal torque. In this work, we show that, for the circular torque given by Kushnir et al. (2017), an accurate, approximate, closed form for the dynamical tide in a highly eccentric MS-CO binary can be obtained. Contrary to existing models of dynamical tides (e.g. Vigna-Gómez et al. 2020), our formulation improves in accuracy as the binary eccentricity increases. We give closed forms for both the tidal torque and inspiral rate of such an MS-CO binary.

In Section 2, we review the relevant equations. In Sections 3 and 4, we derive accurate, approximate closed forms for the torque and energy transfer rate in the binary. In Section 5, we apply results to the binary radio pulsar J0045-7319. We conclude and discuss in Section 6.

## 2 SUMMARY OF RELEVANT WORK

### 2.1 Tidal Torque in Massive Stars

We first review the case where the MS-CO binary is circular. Let  $M_2$  be the mass of the CO,  $a$  be the semimajor axis of the binary, and  $\Omega$  the orbital angular frequency of the binary. The tidal torque exerted

on the star by the companion is (Kushnir et al. 2017):

$$T_{\text{circ}}(\omega) = T_0 \operatorname{sgn}(\omega) \left| \frac{\omega}{\Omega} \right|^{8/3}, \quad (1)$$

$$\begin{aligned} T_0 &= \frac{GM_c^2 r_c^5}{a^6} \left( \frac{\Omega}{\sqrt{GM_c/r_c^3}} \right)^{8/3} \left[ \frac{r_c}{g_c} \left( \frac{dN^2}{d \ln r} \right)_{r=r_c} \right]^{-1/3} \\ &\quad \times \frac{\rho_c}{\bar{\rho}_c} \left( 1 - \frac{\rho_c}{\bar{\rho}_c} \right)^2 \left[ \frac{3}{2} \frac{3^{2/3} \Gamma^2(1/3)}{5 \cdot 6^{4/3}} \frac{3}{4\pi} \alpha^2 \right], \\ &\equiv \beta_2 \frac{GM_c^2 r_c^5}{a^6} \left( \frac{\Omega}{\sqrt{GM_c/r_c^3}} \right)^{8/3} \frac{\rho_c}{\bar{\rho}_c} \left( 1 - \frac{\rho_c}{\bar{\rho}_c} \right)^2. \end{aligned} \quad (2)$$

Here,  $\omega \equiv \Omega - 2\Omega_s$  is the tidal forcing frequency,  $\Omega_s$  is the spin of the massive star,  $N$  is the Brünt-Vaisala frequency,  $r$  is the radial coordinate within the star, and  $r_c, M_c, g_c, \rho_c, \bar{\rho}_c$  are the radius of the RCB, the mass contained within the convective core, the gravitational acceleration at the RCB, the stellar density at the RCB, and the average density of the convective core, respectively.  $\alpha$  and  $\beta_2$  are numerical constants defined by Kushnir et al. (2017), where  $\beta_2 \approx 1$  is a good approximation for a large range of stellar models. In Eq. (1), we have written the terms such that  $T_0$  contains all the spin-independent terms.

## 2.2 Perturbation from an Eccentric Companion: Hansen Coefficients

Separately, we review the general procedure for calculating tidal dissipation due to an eccentric perturber. The gravitational potential of an eccentric companion to quadrupolar order can be decomposed as a sum over circular orbits (e.g. Storch & Lai 2013; Vick et al. 2017):

$$U = \sum_{m=-2}^2 U_{2m}(\vec{r}, t), \quad (3)$$

$$\begin{aligned} U_{2m}(\vec{r}, t) &= -\frac{GM_2 W_{2m} r^2}{D(t)^3} Y_{2m}(\theta, \phi) e^{-imf(t)}, \\ &= -\frac{GM_2 W_{2m} r^2}{a^3} Y_{2m}(\theta, \phi) \sum_{N=-\infty}^{\infty} F_{Nm} e^{-iN\Omega t}. \end{aligned} \quad (4)$$

Here,  $(r, \theta, \phi)$  are the radial, polar, and azimuthal coordinates of  $\vec{r}$  respectively,  $W_{2\pm 2} = \sqrt{3}\pi/10$ ,  $W_{2\pm 1} = 0$ ,  $W_{20} = -\sqrt{\pi}/5$ ,  $D(t)$  is the instantaneous distance between the star and companion,  $f$  is the true anomaly,  $Y_{lm}$  denote the spherical harmonics, and  $\Omega$  is the mean motion of the companion.  $F_{Nm}$  denote the *Hansen coefficients* for  $l = 2$  (also denoted  $X_{2m}^n$  in Murray & Dermott 1999), which are defined implicitly in Eq. (4) to be the Fourier coefficients of the perturbing function, i.e.

$$\frac{a^3}{D(t)^3} e^{-imf(t)} = \sum_{N=-\infty}^{\infty} F_{Nm} e^{-iN\Omega t}. \quad (5)$$

The  $F_{Nm}$  can be written explicitly as an integral over the eccentric anomaly (Murray & Dermott 1999; Storch & Lai 2013), but this requires separate integral for each  $N$ . Instead, taking a discrete Fourier Transform of the left hand side of Eq. (5) permits computation of arbitrarily many  $N$  at once (as pointed out by Correia et al. 2014), which is what is done in this work.

By considering the effect of each summand in Eq. (4), the total torque on the star, energy transfer in the inertial frame, and heating

in the star's corotating frame can be obtained (Storch & Lai 2013; Vick et al. 2017):

$$T = \sum_{N=-\infty}^{\infty} F_{N2}^2 T_{\text{circ}}(N\Omega - 2\Omega_s), \quad (6)$$

$$\begin{aligned} \dot{E}_{\text{in}} &= \frac{1}{2} \sum_{N=-\infty}^{\infty} \left\{ \left( \frac{W_{20}}{W_{22}} \right)^2 N\Omega F_{N0}^2 T_{\text{circ}}(N\Omega) \right. \\ &\quad \left. + N\Omega F_{N2}^2 T_{\text{circ}}(N\Omega - 2\Omega_s) \right\}, \end{aligned} \quad (7)$$

$$\dot{E}_{\text{rot}} = \dot{E}_{\text{in}} - \Omega_s T. \quad (8)$$

## 2.3 Objective of This Paper

The objective of this paper is to study the effect of dynamical tides in an eccentric MS-CO binary. First, we compute the tidal torque by substituting the torque due to a CO on a circular orbit [Eq. (1)] into the summation Eq. (6), obtaining

$$T = \sum_{N=-\infty}^{\infty} F_{N2}^2 T_0 \operatorname{sgn} \left( N - \frac{2\Omega_s}{\Omega} \right) \left| N - \frac{2\Omega_s}{\Omega} \right|^{8/3}. \quad (9)$$

The energy transfer rate in the inertial frame is similarly obtained by substituting Eq. (1) into Eq. (7)

$$\begin{aligned} \dot{E}_{\text{in}} &= \frac{T_0}{2} \sum_{N=-\infty}^{\infty} \left[ N\Omega F_{N2}^2 \operatorname{sgn}(N - 2\Omega_s/\Omega) |N - 2\Omega_s/\Omega|^{8/3} \right. \\ &\quad \left. + \left( \frac{W_{20}}{W_{22}} \right)^2 \Omega F_{N0}^2 |N|^{11/3} \right]. \end{aligned} \quad (10)$$

These two expressions give the spin synchronization timescale of the star as well as the inspiral time of the binary due to dynamical tides. While exact, these expressions are difficult to evaluate for larger eccentricities, where one often must sum hundreds or thousands of terms, each of which has a different  $F_{Nm}$ . In the subsequent sections, our objective is to obtain closed-form approximations to Eqs. (9–10).

## 3 APPROXIMATING HANSEN COEFFICIENTS

In this section, we derive scalings for the Hansen coefficients in the high-eccentricity limit. Since  $F_{(-N)m} = F_{Nm}$ , so we will only study the Hansen coefficient behavior for  $m \geq 0$ .

### 3.1 $m = 2$ Hansen Coefficient Behavior at High Eccentricity

We first consider the case where  $m = 2$ . Figure 1 shows the  $F_{N2}$  for  $e = 0.9$ . First, we note that  $F_{N2}$  is much larger when  $N \geq 0$  than for  $N < 0$ , so we focus on the behavior for  $N \geq 0$ . Here,  $F_{N2}$  has only one substantial peak. There are two characteristic frequency scales,  $\Omega$  and  $\Omega_p$  the pericenter frequency, defined by

$$\Omega_p \equiv \Omega \frac{\sqrt{1+e}}{(1-e)^{3/2}}. \quad (11)$$

For convenience, we also define

$$N_p \equiv \lfloor \Omega_p / \Omega \rfloor, \quad (12)$$

Since  $N_p$  is the largest harmonic scale, we expect that the peak of the  $F_{N2}$  should occur at  $\sim N_p$ . When  $N \gg N_p$ , the Fourier coefficients must fall off exponentially by the Paley-Wiener theorem since the left hand side of Eq. (5) is smooth. On the other hand, when  $N \ll N_p$ ,

since there are no characteristic frequencies between  $\Omega$  and  $\Omega_p$ , we expect that the Hansen coefficients must be scale free between  $N = 1$  and  $N_p$ , i.e. a power law. Both of these characteristics are reflected in Fig. 1.

Motivated by these considerations, we assume the Hansen coefficients can be approximated by

$$F_{N2} \approx \begin{cases} C_2 N^p e^{-N/\eta_2} & N \geq 0, \\ 0 & N < 0, \end{cases} \quad (13)$$

for some fitting coefficients  $C_2$ ,  $p$ , and  $\eta_2$ . By performing fits to  $F_{N2}$ , we found that  $p \approx 2$  is relatively constant for modest-to-large large eccentricities<sup>1</sup>. For the remainder of this work, we take  $p = 2$  to be fixed.

To constrain the remaining two free parameters  $\eta_2$  and  $C_2$  the normalization, we use the well known Hansen coefficient moments (Hut 1981)

$$\sum_{N=-\infty}^{\infty} F_{N2}^2 = \frac{f_5}{(1-e^2)^{9/2}}, \quad (14)$$

$$f_5 \equiv 1 + 3e^2 + \frac{3e^4}{8}, \quad (15)$$

$$\sum_{N=-\infty}^{\infty} F_{N2}^2 N = \frac{2f_2}{(1-e^2)^6}, \quad (16)$$

$$f_2 \equiv 1 + \frac{15e^2}{2} + \frac{45e^4}{8} + \frac{5e^6}{16}. \quad (17)$$

This fixes

$$\eta_2 = \frac{4f_2}{5f_5(1-e^2)^{3/2}}, \quad (18)$$

$$C_2^2 \eta_2^5 = \frac{4f_5}{3(1-e^2)^{9/2}}. \quad (19)$$

Despite having zero free parameters, this formula accurately describes the  $F_{N2}$  as can be seen in Fig. 1.

### 3.2 $m = 0$ Hansen Coefficient Behavior at High Eccentricity

We now turn to the  $m = 0$  Hansen coefficients,  $F_{N0}$ , which are shown in Fig. 2. We know that  $F_{N0} = F_{(-N)0}$ , so we consider only  $N \geq 0$ . From the figure, we see that the  $F_{N0}$  decay exponentially. By dimensional analysis, this decay must occur over scales  $\sim N_p$ . Therefore, we naturally assume the  $F_{N0}$  scale as

$$F_{N0} = C_0 e^{-|N|/\eta_0}. \quad (20)$$

<sup>1</sup> This can be understood, as the left hand side of Eq. (5) resembles the second derivative of a Dirac delta when the eccentricity is substantial: it is sharply peaked about  $t = 0$ , is periodic with period  $P = 2\pi/\Omega$ , and has zero derivative three times every period (at  $t = \epsilon$ ,  $t = P/2$ , and  $t = P - \epsilon$  for some small  $\epsilon \sim \Omega_p^{-1}$ ). This characteristics suggest that it resembles the second derivative of a Gaussian with width  $\sim \Omega_p^{-1}$ . For timescales  $\gtrsim \Omega_p^{-1}$ , this Gaussian further resembles the Dirac delta function, which has a flat Fourier spectrum ( $\propto N^0$ ). Since time differentiation multiplies by  $N$  in frequency space, we see indeed that  $F_{N2} \propto N^2$  for  $N \lesssim N_p$ .

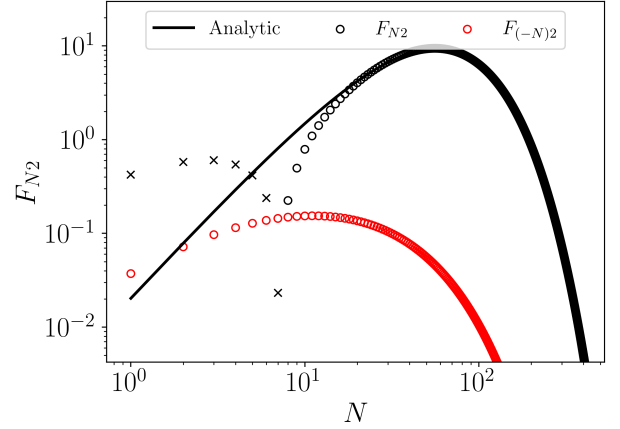


**Figure 1.** Plot of Hansen coefficients  $F_{N2}$  for  $e = 0.9$ . The red dots denote negative  $N$ , while the black dots and crosses denote positive and negative  $F_{N2}$ . The green line is the formula given by Eq. (13) with  $\eta_2$  and  $C_2$  given by Eqs. (18–19).

The two free parameters  $C_0$  and  $\eta_0$  are constrained by the well known moments (Hut 1981)

$$\sum_{N=-\infty}^{\infty} F_{N0}^2 = \frac{f_5}{(1-e^2)^{9/2}}, \quad (21)$$

$$\sum_{N=-\infty}^{\infty} F_{N0}^2 N^2 = \frac{9e^2}{2(1-e^2)^{15/2}} f_3, \quad (22)$$

$$f_3 = \frac{1}{2} + \frac{15e^2}{8} + \frac{15e^4}{16} + \frac{5e^6}{128}. \quad (23)$$

We have defined the common functions  $f_3$  and  $f_5$ . This then requires

$$\eta_0^2 = \frac{9e^2 f_3}{(1-e^2)^3 f_5}, \quad (24)$$

$$C_0^2 \eta_0 = \frac{f_5}{(1-e^2)^{9/2}}. \quad (25)$$

The good agreement of this analytic formula can be seen in Fig. 2.

## 4 EVALUATING TORQUE AND ENERGY TRANSFER

Having found good approximations for the Hansen coefficients, we now apply them to simplify the formulas for the torque and the energy transfer rate in Section 2.3.

### 4.1 Tidal Torque

Towards simplifying the torque, given by Eq. (9), we replace  $F_{N2}$  with Eq. (13) and the sum with an integral, obtaining

$$T = T_0 \int_0^\infty C_2^2 N^4 e^{-2N/\eta_2} \operatorname{sgn}(N - 2\Omega_s/\Omega) |N - 2\Omega_s/\Omega|^{8/3} dN. \quad (26)$$

To further simplify this expression, we analyze it in the large and small spin limits. To distinguish between the two limits, we first define  $N_{\max}$  to be the  $N$  for which the integrand in Eq. (26) is largest assuming  $\Omega_s = 0$ , so  $N_{\max} = 10\eta_2/3$ . Note that if  $\Omega_s$  is large instead,

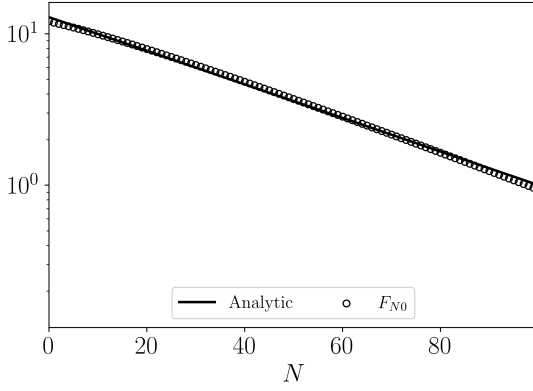


**Figure 2.** Plot of  $F_{N0}$  for  $e = 0.9$ . Since  $F_{N0} = F_{(-N)0}$ , we only show positive  $N$ . The green line is given by Eq. (20) with  $\eta_0$  and  $C_0$  given by Eqs. (24–25).

the integrand is maximized at  $2\eta_2 \simeq N_{\max}$ . The large-spin limit is then where  $|\Omega_s| \gg N_{\max}\Omega/2$ . In this limit, Eq. (9) can be evaluated directly with the known Hansen coefficient moments, which gives

$$\lim_{\Omega_s \rightarrow \infty} T = -T_0 \operatorname{sgn}(\Omega_s) |2\Omega_s/\Omega|^{8/3} \frac{f_5}{(1-e^2)^{9/2}}. \quad (27)$$

The accuracy of this formula is shown in the top panel of Fig. 3 for  $\Omega_s/\Omega = 400 \gg N_{\max}$ . For comparison, we also illustrate the torque predicted by direct integration of Eq. (9). It is seen that both the integral approximation and the asymptotic closed form match the direct summation of Hansen coefficients accurately.

We can also evaluate the small spin limit  $|\Omega_s| \ll N_{\max}\Omega/2$ . Eq. (26) can be integrated analytically<sup>2</sup>, giving

$$\lim_{\Omega_s \rightarrow 0} T = T_0 \frac{f_5(\eta_2/2)^{8/3}}{(1-e^2)^{9/2}} \frac{\Gamma(23/3)}{4!}. \quad (28)$$

The accuracy of this formula is shown in the bottom panel of Fig. 3 for  $\Omega_s/\Omega = 0$ . Again, both the integral approximation and the asymptotic closed form accurately track the explicit sum.

We now have the asymptotic forms of Eq. (26) for large and small spins, but we can derive an approximation valid for all spins. To do this, we first analyze the regime where the spin is small but non-negligible. In this regime, we approximate

$$N - 2\Omega_s/\Omega \simeq \frac{N}{N_{\max}} \left( N_{\max} - \frac{2\gamma_T \Omega_s}{\Omega} \right), \quad (29)$$

for some free parameter  $\gamma_T$ . Using this, we can integrate Eq. (26), and then  $\gamma_T$  is fixed by requiring our expression reproduce the large spin limit [Eq. (27)] when taking  $|\Omega_s| \rightarrow \infty$ . This procedure thus connects the two asymptotic forms Eq. (27–28), and we obtain

$$T = T_0 \frac{f_5(\eta_2/2)^{8/3}}{(1-e^2)^{9/2}} \operatorname{sgn} \left( 1 - \gamma_T \frac{\Omega_s}{\eta_2 \Omega} \right) \left| 1 - \gamma_T \frac{\Omega_s}{\eta_2 \Omega} \right|^{8/3} \frac{\Gamma(23/3)}{4!}, \quad (30)$$

$$\gamma_T = 4 \left( \frac{4!}{\Gamma(23/3)} \right)^{3/8} \approx 0.691. \quad (31)$$

<sup>2</sup> The key to the success of our approach is that sums of form  $\sum_{n=-\infty}^{\infty} F_{N2}^2 N^p$  can be approximated for non-integer  $p$  in terms of  $\Gamma$ , since  $\int_0^\infty x^p e^{-x} dx = \Gamma(p+1)$ . This is not possible with existing analytical techniques.

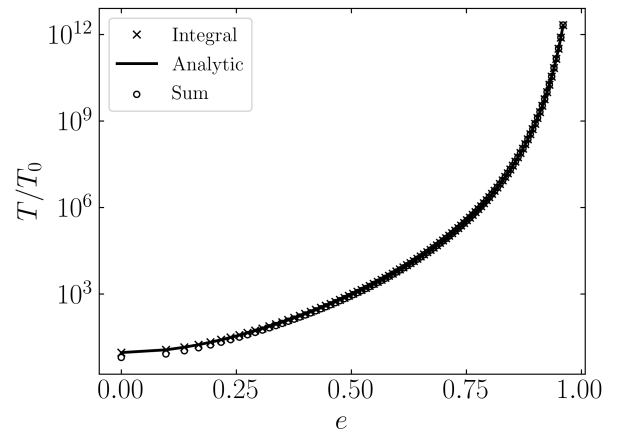
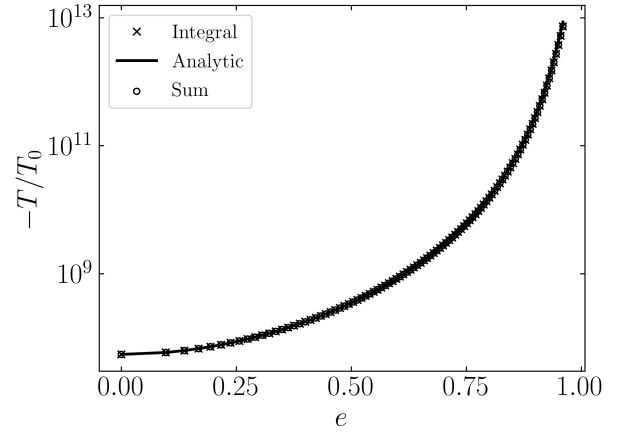


**Figure 3.** Tidal torque on a non-rotating (top) and rapidly rotating ( $\Omega_s/\Omega = 400$ ; bottom) star with a companion having orbital eccentricity  $e$ . Blue plus signs represent explicit summation of Eq. (9), blue crosses are evaluated using the integral approximation Eq. (26), and the green line is Eq. (30). In the large and small spin limits, Eq. (30) reduces to Eq. (27) and Eq. (28) respectively.

Fig. 4 demonstrates the accuracy of this prediction as a function. As expected from the construction of this approximation, both the large and small spin limits are well captured, and the scaling for intermediate spins is also rather accurate. It is worth noting that integration of Eq. (26) is markedly more accurate than the closed form near pseudosynchronization. Note that the integral handles the  $F_{N2}$  approximately but handles the spin dependence exactly. As such, we see that the Hansen coefficient approximations proposed in Section 2 introduce less inaccuracy than the approximations used to evaluate the spin dependence near pseudosynchronization [Eq. (37)].

Finally, the synchronization time can be computed? It's a bit complicated, since dissipation happens in the envelope but is driven by the core. Assuming differential rotation, synchronization is really enforced by magnetic winding or something? Ask Dong

$$\tau_{\text{sync}} = \frac{\Omega_s}{T} k M R^2 \quad (32)$$

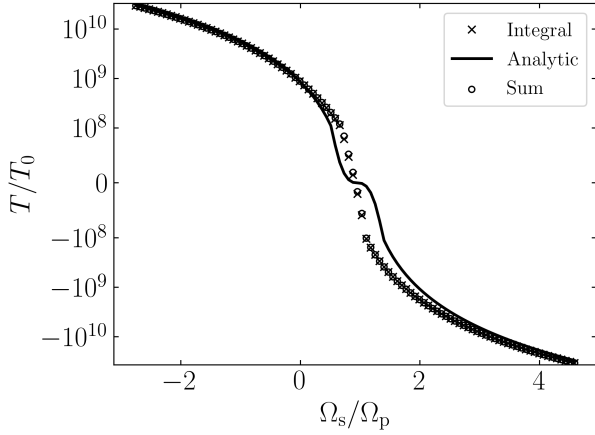


**Figure 4.** Tidal torque as a function of spin for a highly eccentric  $e = 0.9$  companion. Pluses represent direct summation of Hansen coefficients, crosses represent the integral approximation, and solid lines represent the analytic closed form. Blue [red] means positive [negative] torque on the star. The vertical line denotes  $\Omega_s = \Omega_p$ , where  $\Omega_p$  is given by Eq. (11).

#### 4.2 Pseudosynchronization

There is a single  $\Omega_s$  for which the torque, given by Eq. (30), vanishes, which we call the pseudosynchronization spin frequency. It is given by

$$\frac{\Omega_{s,ps}}{\Omega} = \frac{\eta_2}{\gamma_T} = \frac{4f_2}{5\gamma_T f_5 (1-e^2)^{3/2}}. \quad (33)$$

This has the expected scaling  $\Omega_{s,ps} \propto (1-e)^{-3/2} \propto \Omega_p$ . By comparison, in standard weak friction theory of equilibrium tides, the pseudo-synchronized rotation rate is given by (Alexander 1973; Hut 1981)

$$\frac{\Omega_{s,ps}^{(Eq)}}{\Omega} = \frac{f_2}{f_5 (1-e^2)^{3/2}}. \quad (34)$$

This differs from our Eq. (33) by a factor of 1.15. Figure 5 compares these two predictions, as well as  $\Omega_p$ , to applying a root finding algorithm to Eq. (6).  $\Omega_p$  is very nearly equal to  $\Omega_{s,ps}$ , and both are slightly better estimates for the pseudosynchronization spin frequency than  $\Omega_{s,ps}^{(Eq)}$ .

Note that, very near the pseudosynchronized spin frequency, Eq. (30) predicts that  $dT/d\Omega_s \approx 0$ . This is not physically accurate and is an artifact of our factorization ansatz in Eq. (37).

#### 4.3 Closed Form for Energy Transfer

We now turn our attention to Eq. (7) and replace  $F_{N2}$  and  $F_{N0}$  with their approximations [Eqs. (13) and (20)] to obtain

$$\begin{aligned} \dot{E}_{in} = \frac{T_0 \Omega}{2} \int_0^\infty & \left[ C_2^2 N^5 e^{-2N/\eta_2} \text{sgn}(N - 2\Omega_s/\Omega) |N - 2\Omega_s/\Omega|^{8/3} \right. \\ & \left. + 2 \left( \frac{W_{20}}{W_{22}} \right)^2 C_0^2 e^{-2N/\eta_0} N^{11/3} \right] dN. \end{aligned} \quad (35)$$

We evaluate the  $m = 2$  and  $m = 0$  components of this expression separately.

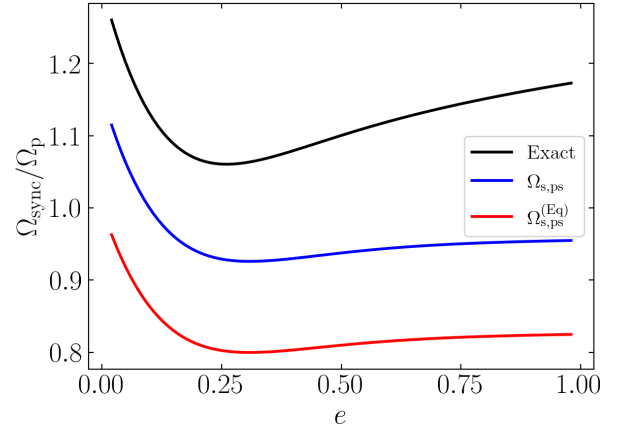


**Figure 5.** Calculations of the pseudosynchronization spin frequencies  $\Omega_{s,sync}$  normalized by the orbital frequency  $\Omega$  as a function of eccentricity (the scale is uniform in  $1-e^2$ ). The green, blue, and red line are given by Eqs. (11), (33), and (34) respectively. The exact solution, given in the black line, is obtained using finding algorithm to solve for the zero of Eq. (6).

We first examine the  $m = 2$  contribution using the same procedure that was used in Section 4.1 for the torque. Here, the integrand is maximized at  $N_{max} = 23\eta_2/6$  when  $\Omega_s = 0$ . In the large spin limit where  $\Omega_s \gg N_{max}\Omega/2$ , the  $m = 2$  contribution evaluates to

$$\lim_{\Omega_s \rightarrow \infty} \dot{E}_{in}^{(m=2)} = -\frac{T_0 \Omega}{2} \text{sgn}(\Omega_s) |2\Omega_s/\Omega|^{8/3} \frac{2f_2}{(1-e^2)^6}. \quad (36)$$

The small spin limit can be similarly computed; it is omitted here for brevity. Instead, we directly seek an approximation valid for all spins, beginning by making the approximation

$$N - 2\Omega_s/\Omega \approx \frac{N}{N_{max}} \left( N_{max} - \frac{2\gamma_E \Omega_s}{\Omega} \right), \quad (37)$$

where  $\gamma_E$  is a free parameter. This lets us integrate the  $m = 2$  component of Eq. (35) analytically, and we can constrain  $\gamma_E$  by requiring the integral agree with Eq. (36). This yields

$$\begin{aligned} \dot{E}_{in}^{(m=2)} = \frac{T_0 \Omega f_5 (\eta_2/2)^{11/3}}{2(1-e^2)^{9/2}} \frac{\Gamma(26/3)}{4!} \\ \times \text{sgn} \left( 1 - \gamma_E \frac{\Omega_s}{\eta_2 \Omega} \right) \left| 1 - \gamma_E \frac{\Omega_s}{\eta_2 \Omega} \right|^{8/3}, \end{aligned} \quad (38)$$

$$\gamma_E = \left( \frac{5! 2^{16/3}}{\Gamma(26/3)} \right)^{3/8} \approx 0.5886. \quad (39)$$

The  $m = 0$  contribution to Eq. (35) is much more straightforward and can be directly integrated using the parameterization Eq. (20). So we obtain the total energy transfer rate

$$\begin{aligned} \dot{E}_{in} = \frac{T_0 \Omega}{2} \left[ \frac{f_5 (\eta_2/2)^{11/3}}{(1-e^2)^{9/2}} \frac{\Gamma(26/3)}{4!} \right. \\ \times \text{sgn} \left( 1 - \gamma_E \frac{\Omega_s}{\eta_2 \Omega} \right) \left| 1 - \gamma_E \frac{\Omega_s}{\eta_2 \Omega} \right|^{8/3} \\ \left. + \frac{f_5 \Gamma(14/3)}{(1-e^2)^{10}} \left( \frac{3}{2} \right)^{8/3} \left( \frac{e^2 f_3}{f_5} \right)^{11/6} \right]. \end{aligned} \quad (40)$$

In Fig. 6, we show the agreement of Eq. (40) in the large and

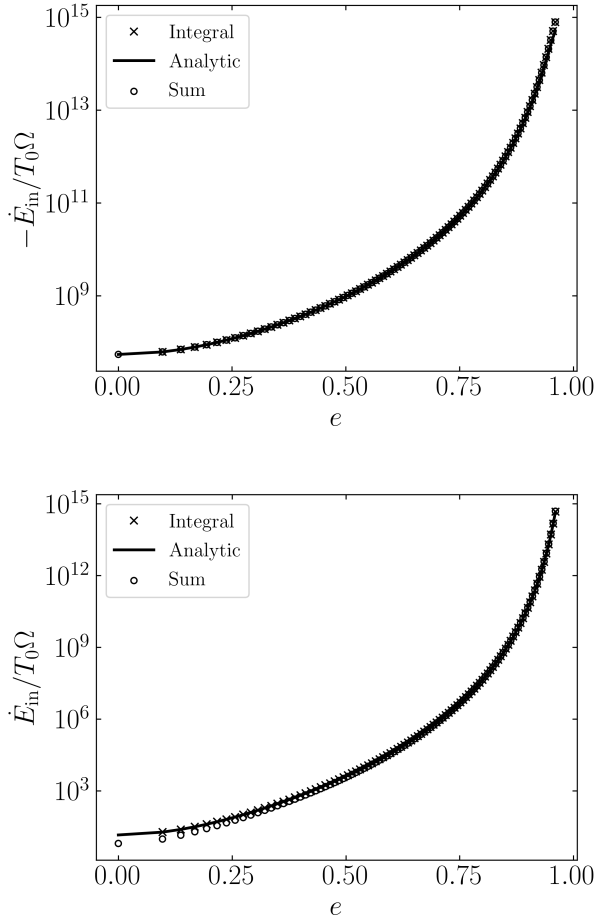


**Figure 6.** Plot of  $\dot{E}_{in}$  for a rapidly rotating ( $\Omega_s/\Omega = 400$ ; top) and non-rotating (bottom) star. Black pluses represent explicit summation of the Hansen coefficients, blue crosses the integral form Eq. (35), and the green line the closed form Eq. (40).

small spin limits, where good agreement is observed both with the integral form Eq. (35) and the closed form Eq. (40). In Fig. 7, we show the energy transfer rate as a function of spin. The agreement degrades near pseudosynchronization but generally captures the correct scaling. Again, explicit integration is visibly more accurate than the analytic closed form.

**With this, a circularization time can also be computed:**

$$\tau_{\text{circ}} = \text{XXXX}. \quad (41)$$

## 5 EXAMPLE SYSTEM: PSR J0045+7319

As an example of our calculations above, we consider PSR J0045-7319 binary system (Bell et al. 1995). The system was initially reported to have pulsar mass  $M_2 = 1.4M_\odot$ ,  $q = 6.3$ ,  $e = 0.808$ , orbital period  $P = 51.17$  days, and  $\dot{P} = -3.03 \times 10^{-7}$  (Kaspi et al. 1996). This gives a mass of  $M = 8.8M_\odot$  for the massive star. Furthermore, the measured luminosity  $L = 1.2 \times 10^4 L_\odot$  and surface temperature  $T_{\text{surf}} = (24000 \pm 1000)$  K give the radius of the star to be  $R = 6.4R_\odot$  (Kaspi et al. 1996).

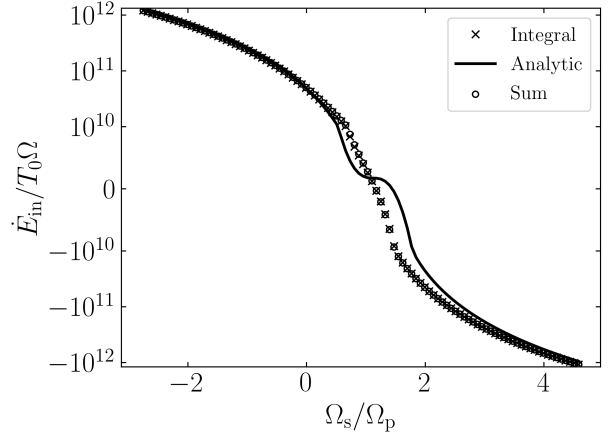


**Figure 7.**  $\dot{E}_{in}$  as a function of spin for a highly eccentric  $e = 0.9$  companion. Pluses represent direct summation of Hansen coefficients, crosses represent the integral approximation, and solid lines represent the analytic closed form. Blue [red] means positive [negative] energy transfer into the spin of the star. The vertical line denotes  $\Omega_s = \Omega_p$ , where  $\Omega_p$  is given by Eq. (11).

## 5.1 Spin of the Massive Star

From these system parameters, we can also calculate the orbital separation  $a = 126R_\odot$ . The internal structure of the star can be obtained by comparison to detailed stellar structure calculations, and yield  $M_c \approx 3M_\odot$  and  $r_c \approx 1.38R_\odot$  (Kumar & Quataert 1998). To account for uncertainties in the stellar structure, we take this  $M_c$  to be fixed and consider a range of  $r_c \in [0.7, 1.5]$ . With these parameters, the spin of the massive star can be computed using our calculations above. By conservation of energy,  $\dot{E}_{in} + \dot{E}_g = 0$ , where  $\dot{E}_g$  is the change in the gravitational binding energy, given by

$$\dot{E}_g = \frac{GqM_2^2}{3a} \frac{\dot{P}}{P}. \quad (42)$$

To relate  $\dot{E}_{in}$  and  $\Omega_s$  to  $\dot{P}$ , we need to make assumptions about the ratio  $\rho_c/\bar{\rho}_c$ , which can only be obtained via stellar structure simulations. We take  $\rho_c/\bar{\rho}_c \approx 1/3$  as a fiducial value (though in reality this likely varies with  $r_c$ ). Figure 8 shows  $|\dot{P}|$  as a function of  $\Omega_s$ , using Eq. (40), evaluated using four different  $r_c$ . The measured  $\dot{P}$  is shown by the horizontal dashed line. Substantial retrograde rotation ( $|\Omega_c| \gg \Omega_p, \sqrt{GM/R^3}$ ) is required to match the predictions. Note furthermore that for the most compact core radius  $r_c = 0.7R_\odot$ , there are no solutions for  $\Omega_s$ ; even a maximally spinning core cannot generate enough tidal dissipation to match the observed  $\dot{P}$ .

## 5.2 Constraints on Stellar Structure

As discovered above, requiring that the observed  $\dot{P}$  lie within the range attainable via tidal dissipation imposes constraints on  $r_c$ . We can compute the range of attainable  $\dot{P}$  by setting the spin frequency equal to the breakup frequency in Eq. (35), giving

$$\dot{P} \lesssim -\frac{6\pi}{q} \beta_2 \left(\frac{r_c}{a}\right)^5 \frac{\rho_c}{\bar{\rho}_c} \left(1 - \frac{\rho_c}{\bar{\rho}_c}\right)^2 2^{8/3} \frac{f_2}{(1-e^2)^6}. \quad (43)$$

For J0045+7319, requiring that  $\dot{P}$  equal its observed value gives  $r_c \gtrsim 0.93R_\odot$  when using  $\rho_c/\bar{\rho}_c = 1/3$ . Indeed, in Fig. 8, there is a solution equal to the observed  $\dot{P}$  when  $r_c \geq R_\odot$  but not when



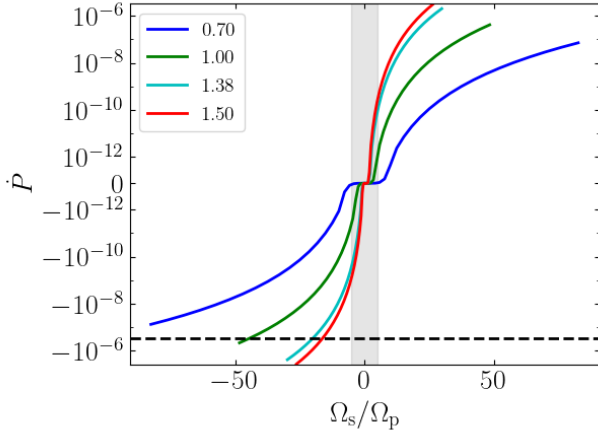


**Figure 8.**  $\dot{P}$  as a function of  $\Omega_s$  for the canonical parameters for J0045-7319, as evaluated by explicit summation of Eq. (10), for four different values of  $r_c$  (legend, in units of  $R_\odot$ ). The measured  $\dot{P} = -3.03 \times 10^{-7}$  is shown by the horizontal dashed line. The vertical shaded region is the region where  $\Omega_s$  is less than the breakup rotation rate of the star as a whole, given by  $\sqrt{GM/R^3}$ . Each  $r_c$  is only shown for  $|\Omega_s| \leq \Omega_{s,c}$  the core breakup rotation rate.

$r_c = 0.7R_\odot$ . The strong dependence of the right hand side on Eq. (43) on  $r_c$  suggests that this constraint is somewhat insensitive to other system uncertainties.

## 6 CONCLUSION AND DISCUSSION

**This section is not complete.**

The primary results of the paper are approximate expressions for the torque, Eq. (30), and the energy dissipation rate, Eq. (40), in closed form.

- Thanks to some references (Barker & Ogilvie, my work), there seems to be some evidence that hydrodynamic wave breaking could cause all IGW to break and not reflect, once the pericenter wave reaches nonlinear amplitudes.
- As noted in the text, the approximate forms enforce  $dT/d\Omega_s = 0$ , which the actual torque does not satisfy. This introduces some slight errors in the exact value of the torque very near pseudosynchronization.
- It is pointed out that the  $v \sin i$  for J0045-7319 is  $110 \pm 10$  km/s, while the breakup frequency is  $\sqrt{GM/R} = 512$  km/s. Thus, it is expected that the stellar surface is rotating at an appreciable fraction of breakup.

## 7 ACKNOWLEDGEMENTS

We thank Michelle Vick, Christopher O'Connor, and Matteo Cantiello for fruitful discussions. YS is supported by the NASA FINESST grant 19-ASTRO19-0041.

## REFERENCES

- Alexander M., 1973, *Astrophysics and Space Science*, 23, 459  
 Bell J., Bessell M., Stappers B., Bailes M., Kaspi V., 1995, *The Astrophysical Journal Letters*, 447, L117

- Correia A. C., Boué G., Laskar J., Rodríguez A., 2014, *Astronomy & Astrophysics*, 571, A50  
 Goldreich P., Nicholson P. D., 1989, *Astrophysical Journal*, 342, 1079  
 Hurley J. R., Tout C. A., Pols O. R., 2002, *Monthly Notices of the Royal Astronomical Society*, 329, 897  
 Hut P., 1981, *Astronomy and Astrophysics*, 99, 126  
 Kaspi V., Bailes M., Manchester R., Stappers B., Bell J., 1996, *Nature*, 381, 584  
 Kumar P., Quataert E. J., 1998, *The Astrophysical Journal*, 493, 412  
 Kushnir D., Zaldarriaga M., Kollmeier J. A., Waldman R., 2017, *Monthly Notices of the Royal Astronomical Society*, 467, 2146  
 Murray C. D., Dermott S. F., 1999, *Solar system dynamics*. Cambridge university press  
 Savonije G., Papaloizou J., 1983, *Monthly Notices of the Royal Astronomical Society*, 203, 581  
 Storch N. I., Lai D., 2013, *Monthly Notices of the Royal Astronomical Society*, 438, 1526  
 Vick M., Lai D., Fuller J., 2017, *Monthly Notices of the Royal Astronomical Society*, 468, 2296  
 Vigna-Gómez A., MacLeod M., Neijssel C. J., Broekgaarden F. S., Justham S., Howitt G., de Mink S. E., Mandel I., 2020, *arXiv preprint arXiv:2001.09829*  
 Zahn J.-P., 1975, *Astronomy and Astrophysics*, 41, 329

This paper has been typeset from a  $\text{\LaTeX}$  file prepared by the author.